LETTER

doi:10.1038/nature13795

Identification of an iridium-containing compound with a formal oxidation state of IX

Guanjun Wang[1], Mingfei Zhou[1], James T. Goettel[2], Gary J. Schrobilgen[2], Jing Su[3], Jun Li[3], Tobias Schlöder[4] & Sebastian Riedel[4,5]

One of the most important classifications in chemistry and within the periodic table is the concept of formal oxidation states[1–4]. The preparation and characterization of compounds containing elements with unusual oxidation states is of great interest to chemists[5]. The highest experimentally known formal oxidation state of any chemical element is at present VIII[2–4], although higher oxidation states have been postulated[6,7]. Compounds with oxidation state VIII include several xenon compounds[8] (for example XeO_4 and XeO_3F_2) and the well-characterized species RuO_4 and OsO_4 (refs 2–4). Iridium, which has nine valence electrons, is predicted to have the greatest chance of being oxidized beyond the VIII oxidation state[1]. In recent matrix-isolation experiments, the IrO_4 molecule was characterized as an isolated molecule in rare-gas matrices[9]. The valence electron configuration of iridium in IrO_4 is $5d^1$, with a formal oxidation state of VIII. Removal of the remaining *d* electron from IrO_4 would lead to the iridium tetroxide cation ($[IrO_4]^+$), which was recently predicted to be stable[10] and in which iridium is in a formal oxidation state of IX. There has been some speculation about the formation of $[IrO_4]^+$ species[11,12], but these experimental observations have not been structurally confirmed. Here we report the formation of $[IrO_4]^+$ and its identification by infrared photodissociation spectroscopy. Quantum-chemical calculations were carried out at the highest level of theory that is available today, and predict that the iridium tetroxide cation, with a T_d-symmetrical structure and a d^0 electron configuration, is the most stable of all possible $[IrO_4]^+$ isomers.

Iridium oxide cations were generated in the gas phase using a pulsed-laser vaporization/supersonic-expansion source and were studied by infrared photodissociation spectroscopy in the 850–1,600 cm^{-1} region as described previously[13]. A typical mass spectrum of the iridium oxide cations produced with O_2-seeded helium is shown in Fig. 1a. The spectrum consists of a progression of peaks having different masses that correspond to different $[IrO_x]^+$ species with up to six oxygen atoms. Enhanced abundance in the mass spectrum was found for $[IrO_4]^+$, and the preferential formation of this cation indicates increased stability. Because the dissociation energies of the $[IrO_4]^+$ cations are significantly greater than the infrared photon energies in the Ir=O and O–O stretching frequency region (the infrared photons in the 900–1,200 cm^{-1} region have energies in the range of 10.8–14.4 kJ mol^{-1}; Supplementary Information), the method of rare-gas atom predissociation is employed to obtain the infrared spectra for these molecules[14–17]. When argon was used instead of helium, $[IrO_4]^+ \cdot Ar_n$ ions ($n = 1$, 2 and larger; the dot denotes a weak bond) were produced (Fig. 1b) and the mass peaks corresponding to the $[^{193}IrO_4]^+ \cdot Ar_n$ isotopomers were selected for photodissociation. When the infrared laser is on resonance with one of the vibrational fundamentals of an $[IrO_4]^+ \cdot Ar_n$ complex, the latter photodissociates by eliminating an argon atom. The resulting predissociation infrared spectra of $[IrO_4]^+$ are shown in Fig. 2.

The experimental spectrum of $[IrO_4]^+ \cdot Ar$ (Fig. 2a) consists of five absorptions at 936, 944, 966, 1,047 and 1,054 cm^{-1}, respectively, (Table 1), indicating that more than one isomer is experimentally observed, because any $[IrO_4]^+$ structure should at most have four vibrational fundamentals in the Ir=O and O–O stretching regions. Experiments with different time delays between expansion from the pulsed valve and vaporization (Methods), and with different stagnation pressures, suggest that the bands at 936 and 944 cm^{-1} are due to the same species, whereas the other three absorptions are caused by other isomers. All bands were shifted to lower wavenumbers in the experiments using $^{18}O_2$ (Supplementary Information), and the observed frequency shifts with $^{16}O/^{18}O$ isotopic ratios in the range of 1.050–1.056 suggest that these bands originate from Ir=O or O−O stretching vibrations.

Recent quantum-chemical calculations show that three low-energy isomers are possible for a cation of $[IrO_4]^+$ stoichiometry[10]. These cations have been reinvestigated by more accurate *ab initio* coupled-cluster calculations with single and double excitations and perturbative-triples corrections (CCSD(T)), as well as by *ab initio* multi-reference-based complete active space perturbation theory (CASPT2) calculations (Methods). On the basis of these calculations, the wavenumber of the O−O stretching mode of the superoxide complex is predicted to be 1,486.3 cm^{-1} at density functional level with inclusion of dispersion corrections (B3LYP-D3) or 1,458.7 cm^{-1} (CCSD(T)) with appreciable infrared intensity. Hence, this superoxide complex $[(\eta^1\text{-}O_2)Ir^{VI}O_2]^+$ (C_s symmetry, $^3A''$ ground state) can be ruled out because of the absence of any observed band in the experimental spectra above 1,100 cm^{-1}. The observed absorptions probably come from the side-on O_2 complex $[(\eta^2\text{-}O_2)Ir^{VII}O_2]^+$ (C_{2v}, $^1A_1$) and the tetroxide complex $[Ir^{IX}O_4]^+$ (T_d, $^1A_1$), where the

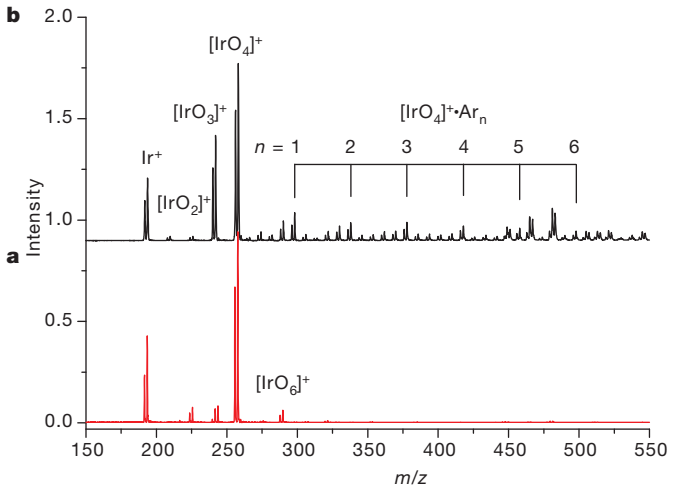

Figure 1 | Mass spectra of the iridium oxide cations. The cations are produced by pulsed-laser vaporization of an iridium metal target in an expansion of helium (**a**) or argon (**b**) seeded by dioxygen. The isotopic splitting of iridium can clearly be resolved with the relative peak areas matching the natural abundance isotopic distribution (^{191}Ir, 37.3%; ^{193}Ir, 62.7%). *m/z*, mass/charge ratio; intensity is shown in arbitrary units.

[1]Collaborative Innovation Center of Chemistry for Energy Materials, Department of Chemistry, Shanghai Key Laboratory of Molecular Catalysts and Innovative Materials, Fudan University, Shanghai 200433, China. [2]Department of Chemistry, McMaster University, 1280 Main Street West, Hamilton, Ontario L8S 4M1, Canada. [3]Department of Chemistry and Key Laboratory of Organic Optoelectronics and Molecular Engineering of Ministry of Education, Tsinghua University, Beijing 100084, China. [4]Institut für Anorganische und Analytische Chemie, Albert-Ludwigs Universität Freiburg, Albertstrasse 21, D-79104 Freiburg im Breisgau, Germany. [5]Institut für Chemie und Biochemie – Anorganische Chemie, Freie Universität Berlin, Fabeckstrasse 34-36, D-14195 Berlin, Germany.

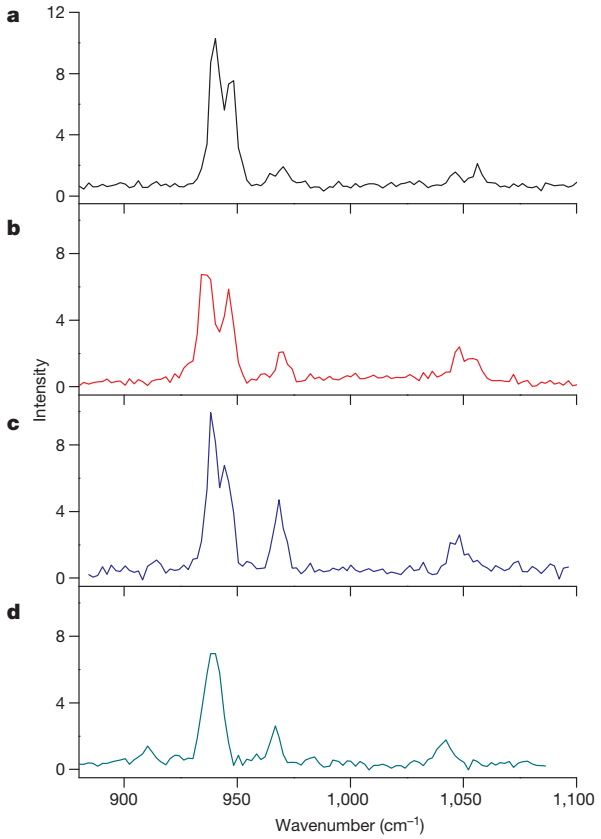

Figure 2 | Infrared photodissociation spectra of the $[^{193}IrO_4]^+ \cdot Ar_n$ ($n = 1$–4) cations. The spectra are measured by monitoring the Ar photodissociation channel: **a**, $[^{193}IrO_4]^+ \cdot Ar$; **b**, $[^{193}IrO_4]^+ \cdot Ar_2$; **c**, $[^{193}IrO_4]^+ \cdot Ar_3$; **d**, $[^{193}IrO_4]^+ \cdot Ar_4$. Intensity is shown as the yield of fragmentation ions normalized to the parent ion signal in percentage.

latter is by far the most stable isomer according to high-level (coupled-cluster) calculations (Fig. 3).

Following the general rules for the determination of formal oxidation states, the experimentally identified cation $[IrO_4]^+$ can be viewed as an Ir(IX) species. This assignment is in line with the well-known isoelectronic OsO_4 molecule, in which osmium undoubtedly exists in its oxidation state VIII. A more detailed discussion of the assignment of oxidation states based on natural population analysis and molecular orbitals is provided in Methods.

Table 1 | Observed and calculated vibrational frequencies of the $[IrO_4]^+$ and the face-coordinated C_{3v} $[IrO_4]^+ \cdot Ar$ isomers

Isomer	$[IrO_4]^+$ (cm^{-1})		$[IrO_4]^+ \cdot Ar$ (cm^{-1})			Mode*
	CCSD(T)†	B3LYP†	CCSD(T)†	B3LYP†	Exptl	
$[IrO_4]^+$	916.4 (0)	1,009.8 (0)	916.7 (0)	1,008.9 (0)	936	Sym. str. (A_1)
	963.0 (35)	1,008.5 (39)	963.3 (13)	1,007.5 (40)		Antisym. str. (T_2)
	963.0 (35)	1,008.5 (39)	963.5 (11)	1,009.0 (39)	944	Antisym. str. (T_2)
	963.0 (35)	1,008.5 (39)	963.5 (11)	1,009.0 (39)		Antisym. str. (T_2)
$[(\eta^2\text{-}O_2)IrO_2]^+$	954.9 (55)	1,026.8 (70)	—	1,025.0 (72)	966	OIrO antisym. str. (B_1)
	1,000.6 (11)	1,062.7 (12)	—	1,061.9 (19)	1,047	OIrO sym. str. (A_1)
	996.5 (56)	1,032.8 (60)	—	1,027.9 (59)	1,054	O–O str. (A_1)

Infrared intensities are listed in parentheses in km mol^{-1}.
* Mode descriptions and symmetry labels for the free cations.
† Calculated at CCSD(T)/aug-cc-pVTZ-PP and B3LYP-D3/aug-cc-pVTZ-PP levels. The frequencies of the edge-coordinated (η^2) C_{2v} structure are predicted at 916.8 cm^{-1} (0 km mol^{-1}, A_1), 963.0 cm^{-1} (12 km mol^{-1}, A_1), 963.4 cm^{-1} (10 km mol^{-1}, B_2), 963.6 cm^{-1}(12 km mol^{-1}, B_1) at the CCSD(T) level.
All experiments have been replicated more than ten times.

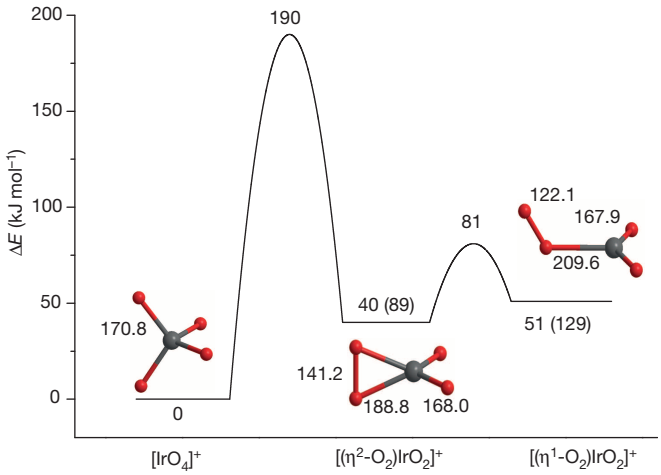

Figure 3 | Optimized structures and energetic ordering of the different $[IrO_4]^+$ isomers. The structures are optimized at the CCSD(T) level. The barriers of the interconversion reactions are also shown. The relative energies are calculated at the SO-DFT/B3LYP and CCSD(T) (in parentheses) levels, with the energy of the most stable isomer ($[IrO_4]^+$) set to zero. The symmetries and ground states are as follows: $[IrO_4]^+$ (T_d, $^1A_1$), $[(\eta^2\text{-}O_2)IrO_2]^+$ (C_{2v}, $^1A_1$), $[(\eta^1\text{-}O_2)IrO_2]^+$ (C_s, $^3A''$). Bond lengths are in pm; energies are in kJ mol^{-1}. Red, oxygen atoms; grey, iridium atoms.

The second most stable isomer of $[IrO_4]^+$ stoichiometry is the C_{2v}-symmetrical side-on complex $[(\eta^2\text{-}O_2)Ir^{VII}O_2]^+$, which was also calculated to have a closed-shell electron configuration. All three isomers were calculated to be true minima on the potential energy surface and are energetically separated by 89 and 40 kJ mol^{-1}, respectively, at the CCSD(T) level (Fig. 3). Our calculations show that their energetic ordering is not affected by weak argon coordination (Supplementary Information). The barrier for the $[(\eta^1\text{-}O_2)IrO_2]^+ \rightarrow [(\eta^2\text{-}O_2)IrO_2]^+$ conversion was calculated to be only about 30 kJ mol^{-1} using density functional theory with relativistic spin–orbit coupling effects (SO-DFT/B3LYP; Fig. 3 and Supplementary Information). The barrier for the $[(\eta^2\text{-}O_2)IrO_2]^+ \rightarrow [IrO_4]^+$ reaction lies at 150 kJ mol^{-1} at the SO-DFT/B3LYP level (Fig. 3 and Supplementary Information). This barrier is remarkably high, but nevertheless is plausible because the isomerization reaction involves the electron transfer and cleavage of the relatively strong peroxide O–O bond[18]. The $[Ir(\eta^2\text{-}O_2)]^+ \rightarrow [IrO_2]^+$ isomerization reaction was computed to have a comparable barrier[19].

From comprehensive analysis and quantum-chemical calculations, we assign the 936 and 944 cm^{-1} bands to the antisymmetric iridium oxide stretching modes of the argon-tagged iridium tetroxide cation (Table 1 and Fig. 2a). Only the triply degenerate antisymmetric stretching mode (T_2 mode) is infrared-active in the tetrahedral $[IrO_4]^+$ cation. In the experimental spectrum of $[IrO_4]^+ \cdot Ar$, we identified two bands separated by 8 cm^{-1} using argon-atom tagging. Our theoretical calculations on all three possible argon coordination modes to $[IrO_4]^+$, namely face coordination (η^3, C_{3v}), edge coordination (η^2, C_{2v}) and vertex coordination (η^1, C_{3v}), show that only the face- and edge-coordinated isomers are stable, with the face-coordinated isomer being slightly more stable than the edge-coordinated isomer (2.0 kJ mol^{-1} at CCSD(T) and 3.5 kJ mol^{-1} at CASPT2). Therefore, both isomers may coexist under the experimental conditions. As a result of symmetry reduction by argon coordination, the triple degeneracy of the antisymmetric iridium oxide stretching modes is lifted, and the T_2 mode splits into distinct modes. Calculations at the B3LYP and CCSD(T) levels show very small mode splitting (0.2 cm^{-1} at CCSD(T), 1.5 cm^{-1} at B3LYP-D3 and 2.0 cm^{-1} at SO-DFT/B3LYP for the face-coordinated isomer) because the predicted O···Ar distances are quite large and the $[IrO_4]^+$ moiety in $[IrO_4]^+ \cdot Ar$ has essentially the same structure as the free cation. Additional *ab initio* multi-reference-based CASPT2 calculations found that there are multi-reference features in $[IrO_4]^+$ and $[IrO_4]^+ \cdot Ar$. The optimized structures (Supplementary Information) show that the O···Ar distances are reduced by comparison

with single-reference methods and that the IrO_4 fragment exhibits some structural distortion from tetrahedral symmetry, which will surely cause a larger mode splitting than is calculated at the B3LYP and CCSD(T) levels of theory.

Further evidence for the above assignment is gained from additional argon atom coordination. The infrared spectra of the $[IrO_4]^+\cdot Ar_n$ cations with $n = 2$–4 are shown in Fig. 2b–d. Owing to symmetry reduction, further mode splitting is observed in the case of $[IrO_4]^+\cdot Ar_2$, where the lower-wavenumber band is broad, suggesting the presence of unresolved bands. The spectrum of $[IrO_4]^+\cdot Ar_3$ shown in Fig. 2c is about the same as that of the single-argon-coordinated complex because the $[IrO_4]^+$ cation of the $[IrO_4]^+\cdot Ar_3$ complex can retain the same symmetry as the $[IrO_4]^+$ cation in $[IrO_4]^+\cdot Ar$. If the experimental conditions are varied, a spectrum involving three distinct bands at 928, 938 and 944 cm^{-1} can clearly be resolved for the $[IrO_4]^+\cdot Ar_3$ cation, suggesting that additional isomers with mixed coordination modes can be formed (Supplementary Information). When four argon atoms were tagged, only one band at 939 cm^{-1} was observed in the spectrum of the $[IrO_4]^+\cdot Ar_4$ cation (Fig. 2d). In this complex, the tetrahedral symmetry of $[IrO_4]^+$ is retained, and so no splitting due to symmetry reduction is expected.

Apart from the bands assigned to the iridium tetroxide cation, three additional absorptions in the experimental spectrum of $[IrO_4]^+\cdot Ar$ were attributed to different vibrational modes of the $[(\eta^2\text{-}O_2)IrO_2]^+$ complex (Table 1 and Fig. 3). The assignment of the 1,054 cm^{-1} band to the O−O stretching vibration is consistent with the identification of $[(\eta^2\text{-}O_2)IrO_2]^+$ as a cationic peroxide complex[20]. The unprecedented Ir(VII) oxidation state of $[(\eta^2\text{-}O_2)IrO_2]^+$ now closes the gap between the well-known VI and the recently discovered VIII[9] oxidation states of this metal. Further evidence for the assignment of the vibrational bands is provided by comparison with the isoelectronic compounds OsO_4 and $[(\eta^2\text{-}O_2)OsO_2]$ previously investigated by matrix-isolation spectroscopy[21] (Supplementary Information). Although this $[(\eta^2\text{-}O_2)IrO_2]^+$ complex was predicted at CCSD(T) level to be 89 kJ mol^{-1} higher in energy than the tetroxide cation isomer, both structures were experimentally observed, most probably due to the relatively high barrier for the interconversion between the two isomers (see above). With both the $[(\eta^2\text{-}O_2)Ir^{VII}O_2]^+$ peroxo complex and the $[Ir^{IX}O_4]^+$ tetroxide complex experimentally characterized here, all possible positive oxidation states of iridium ranging from I to IX are now known.

As well as this gas-phase spectroscopic characterization, experimental attempts have been undertaken to isolate iridium compounds in the IX oxidation state. Proposed syntheses of stable $[IrO_4]^+$ salts by the reaction of $[O_2][SbF_6]$ or $[O_2][Al(OC(CF_3)_3)_4]$ with IrO_2 were motivated by the calculated Gibbs free energies (ΔG^o) derived from the appropriate Born–Haber cycles: the reactions forming $[IrO_4][SbF_6]$ and $[IrO_4][Al(OC(CF_3)_3)_4]$ were predicted to be exergonic by −14 and −66 kJ mol^{-1}, respectively[10]. The use of the weakly coordinating anion $[Sb_2F_{11}]^-$ would also be expected to lead to an exergonic reaction having a ΔG^o value that is intermediate with respect to $[SbF_6]^-$ and $[Al(OC(CF_3)_3)_4]^-$. Considering the possibility of a thermally unstable product, the reactions of $[O_2][Sb_2F_{11}]$ and IrO_2 were initially attempted at low temperatures (−120 to −78 °C) in SO_2ClF and anhydrous HF solvents. The SO_2ClF solution instantly turned bright purple, which was shown to result from the interaction between O_2^+ and SO_2ClF; that is, dissolution of $[O_2][Sb_2F_{11}]$ in SO_2ClF under similar conditions also yielded a bright purple solution. Attempts to synthesize a stable $[IrO_4][Sb_nF_{5n+1}]$ salt by the reaction of $[O_2][Sb_2F_{11}]$ and IrO_2 in superacidic mixtures of HF and SbF_5 also gave purple solutions, but no evidence for $[IrO_4]^+$ was found. The purple solutions are probably attributable to polyoxygen fluoride radicals, $(O_2)_{n+1}F$, as previously described[22]. To further test the oxidizability of IrO_2, the reaction of molten XeF_6 with IrO_2 was attempted to determine whether an iridium oxide fluoride species in a higher oxidation state could be formed. There was no apparent reaction even after heating the reaction mixture to 100 °C for over one hour. However, the addition of anhydrous HF to the aforementioned reaction mixture of IrO_2 and XeF_6 afforded a dark brown solution at 21 °C, from which crystals of $[Xe_2F_{11}][IrF_6]$ were grown. The crystal structure of $[Xe_2F_{11}][IrF_6]$, and related work, will be reported elsewhere. Although IrO_2 reacted with XeF_6, the high lattice enthalpy associated with the rutile structure of IrO_2 may significantly inhibit its reactivity with O_2^+. Details of the aforementioned attempts to synthesize an $[IrO_4]^+$ salt are provided in Supplementary Information.

Online Content Methods, along with any additional Extended Data display items and Source Data, are available in the online version of the paper; references unique to these sections appear only in the online paper.

Received 1 May 2013; accepted 21 August 2014.

1. Jørgensen, C. K. *Oxidation Numbers and Oxidation States* (Springer, 1969).
2. Riedel, S. & Kaupp, M. The highest oxidation states of the transition metal elements. *Coord. Chem. Rev.* **253,** 606–624 (2009).
3. Riedel, S. in *Comprehensive Inorganic Chemistry II* (eds Reedijk, J. & Poeppelmeier, K.) 187–221 (Elsevier, 2013).
4. Schlöder, T. & Riedel, S. in *Comprehensive Inorganic Chemistry* Vol. 9 (ed. Alvarez, S.) 227–243 (Elsevier, 2013).
5. Jørgensen, C. K. New understanding of unusual oxidation states in the transition groups. *Naturwissenschaften* **63,** 292 (1976).
6. Pyykkö, P., Runeberg, N., Straka, M. & Dyall, K. G. Could uranium(XII) hexoxide, UO_6 (O_h) exist? *Chem. Phys. Lett.* **328,** 415–419 (2000).
7. Xiao, H., Hu, H.-S., Schwarz, W. H. E. & Li, J. Theoretical investigations of geometry, electronic structure and stability of UO_6: octahedral uranium hexoxide and its isomers. *J. Phys. Chem. A* **114,** 8837–8844 (2010).
8. Gerken, M. & Schrobilgen, G. J. Solution multi-NMR and Raman spectroscopic studies of thermodynamically unstable XeO_4. The first ^{131}Xe NMR study of a chemically bound xenon species. *Inorg. Chem.* **41,** 198–204 (2002).
9. Gong, Y., Zhou, M., Kaupp, M. & Riedel, S. Formation and characterization of the iridium tetraoxide molecule with iridium in the oxidation state VIII. *Angew. Chem. Int. Ed.* **48,** 7879–7883 (2009).
10. Himmel, D., Knapp, C., Patzschke, M. & Riedel, S. How far can we go? Quantum-chemical investigations of oxidation state IX. *ChemPhysChem* **11,** 865–869 (2010).
11. Rother, P., Wagner, F. & Zahn, U. Chemical consequences of the $^{193}Os(\beta^-)^{193}Ir$ decay in osmium compounds studied by the Mössbauer method. *Radiochim. Acta* **11,** 203–210 (1969).
12. Koyanagi, G. K., Caraiman, D., Blagojevic, V. & Bohme, D. K. Gas-phase reactions of transition-metal ions with molecular oxygen: room-temperature kinetics and periodicities in reactivity. *J. Phys. Chem. A* **106,** 4581–4590 (2002).
13. Wang, G. *et al.* Infrared photodissociation spectroscopy of mononuclear iron carbonyl anions. *J. Phys. Chem. A* **116,** 2484–2489 (2012).
14. Duncan, M. A. Infrared spectroscopy to probe structure and dynamics in metal ion-molecule complexes. *Int. Rev. Phys. Chem.* **22,** 407–435 (2003).
15. Okumura, M., Yeh, L. I., Myers, J. D. & Lee, Y. T. Infrared spectra of the solvated hydronium ion: vibrational predissociation spectroscopy of mass-selected $H_3O^+\cdot(H_2O)_n\cdot(H_2)_m$. *J. Phys. Chem.* **94,** 3416–3427 (1990).
16. Bieske, E. J. & Dopfer, O. High-resolution spectroscopy of cluster ions. *Chem. Rev.* **100,** 3963–3998 (2000).
17. Robertson, W. H. & Johnson, M. A. Molecular aspects of halide ion hydration: the cluster approach. *Annu. Rev. Phys. Chem.* **54,** 173–213 (2003).
18. Bach, R. D., Ayala, P. Y. & Schlegel, H. B. A reassessment of the bond dissociation energies of peroxides. An ab initio study. *J. Am. Chem. Soc.* **118,** 12758–12765 (1996).
19. Armentrout, P. B. & Li, F. X. Bond energy of IrO^+: guided ion-beam and theoretical studies of the reaction of Ir^+ (^5F) with O_2. *J. Phys. Chem. A* **117,** 7754–7766 (2013).
20. Gong, Y., Zhou, M. F. & Andrews, L. Spectroscopic and theoretical studies of transition metal oxides and dioxygen complexes. *Chem. Rev.* **109,** 6765–6808 (2009).
21. Zhou, M. F., Citra, A., Liang, B. Y. & Andrews, L. Infrared spectra and density functional calculations for MO_2, MO_3, $(O_2)MO_2$, MO_4, MO_2^- (M=Re, Ru, Os) and ReO_3^-, ReO_4^- in solid neon and argon. *J. Phys. Chem. A* **104,** 3457–3465 (2000).
22. Christe, K. O., Wilson, R. D. & Goldberg, I. B. Some observations on the reaction chemistry of dioxygenyl salts and on the blue and purple compounds believed to be ClF_3O_2. *J. Fluor. Chem.* **7,** 543–549 (1976).

Supplementary Information is available in the online version of the paper.

Acknowledgements This work was supported by the Ministry of Science and Technology of China (2013CB834603 and 2012YQ220113-3), the National Natural Science Foundation of China (grant nos 21173053, 21433005 and 91026003), the Committee of Science and Technology of Shanghai (13XD1400800), the Fonds der Chemischen Industrie and the GRK 1582 'Fluorine as a key element'. We also acknowledge the Natural Sciences and Engineering Research Council of Canada for a Discovery Grant (G.J.S.) and for a postgraduate scholarship (J.T.G.). We are grateful to I. Krossing and H. Hillebrecht for their support.

Author Contributions G.W. and M.Z. designed and performed the gas-phase experiments, J.T.G. and G.J.S. attempted to synthesize $[IrO_4]$ salts, J.S., J.L., T.S. and S.R. performed the quantum chemical calculations. M.Z., G.J.S., J.L. and S.R. wrote the paper and supervised the experimental and theoretical parts. All authors discussed the results and commented on the manuscript at all stages.

Author Information Reprints and permissions information is available at www.nature.com/reprints. The authors declare no competing financial interests. Readers are welcome to comment on the online version of the paper. Correspondence and requests for materials should be addressed to M.Z. (mfzhou@fudan.edu.cn), G.J.S. (schrobil@mcmaster.ca) or S.R. (sriedel@psichem.de).

METHODS

Experimental details. Iridium oxide cations were generated in the gas phase using a pulsed-laser vaporization/supersonic expansion source. Reactive iridium atoms and cations were generated by the 1,064-nm fundamental of a Nd:YAG laser that was focused onto a rotating iridium metal target. Helium or argon gas, seeded with a few per cent of O_2, was expanded out of a pulsed valve (General Valve, Series 9) at a stagnation pressure of 8−13 atm. The iridium oxide ions and their argon-tagged complexes generated by laser vaporization were collisionally cooled in the expansion. After free expansion, the cations were skimmed into a second differentially pumped chamber, where the cations were pulse-extracted into a collinear tandem time-of-flight mass spectrometer. Ions were mass-selected by their flight times and then studied by infrared laser photodissociation spectroscopy using a tunable infrared optical parametric oscillator/optical parametric amplifier laser system (LaserVision, pumped by a Continuum Powerlite 8000 Nd:YAG laser). The photodissociation spectrum was obtained by monitoring the yields of the fragment ions as a function of the dissociation infrared laser wavelength and normalizing to the parent ion signal.

Theoretical and computational details. The iridium oxides and argon-tagged species were studied by using both density functional theory (DFT) and wave-function-based theory (WFT). The structures of all molecules were fully optimized by relaxing all geometric parameters at the DFT level using the B3LYP functional[23–26]. The choice of this functional was based on its good performance for comparable molecules[27]. To determine the ground states of the molecules, several spin multiplicities were calculated. In the case of the weak argon complexes, an empirical correction for dispersive interactions (D3) was included in the DFT calculations[28]. Further symmetrical stationary points on the potential energy surface were calculated within the restrictions of the given point groups. Dunning's correlation-consistent triple-ζ basis sets (aug-cc-pVTZ) were used for both oxygen and argon atoms[29,30]. Scalar relativistic effects were considered by using relativistic energy-consistent small-core pseudopotentials for the metal atom and the corresponding aug-cc-pVTZ-PP basis sets[31,32]. For brevity, this basis set combination is referred to as aug-cc-pVTZ(-PP). In the DFT calculations, averaged masses were used for all elements if not otherwise noted. All standard DFT calculations were performed with the Gaussian 09 program package[23], whereas the Turbomole V6.4 suite of programs was used for DFT-D3 calculations[33].

Beyond these calculations, the influence of spin–orbit coupling has been investigated for the energy-minimized structures as well as for the energy barriers. To estimate the interstate crossing energy barrier of the transition from the $[IrO_2(\eta^2\text{-}O_2)]^+$ (d^2) singlet to the $[IrO_4]^+$ (d^0) singlet, a series of linear transit calculations were performed by using the DFT/B3LYP method. The starting point of the linear transit energy curves corresponds to the optimized $[IrO_2(\eta^2\text{-}O_2)]^+$ structure and the ending point to the optimized $[IrO_4]^+$ structure. The linear transit total energies were obtained by constrained optimizations at each linear transit coordinate along the distance from Ir to the centre of the η^2-O_2 configuration. The Slater basis sets with the quality of triple-ζ plus two polarization functions[34] were used, with the frozen-core approximation applied to the inner shells $[1s^2-4f^{14}]$ for Ir and $[1s^2]$ for O. In these calculations, the scalar relativistic and spin–orbit effects were taken into account by the zeroth-order regular approximation[35]. With inclusion of scalar relativistic effects, both the singlet and triplet potential energy surfaces were explored. To further investigate the spin–orbit effects, unrestricted Kohn–Sham calculations with a non-collinear spin–orbit approach were also used in the linear transit calculations. These linear transit calculations were done with Amsterdam density functional (ADF 2013.01) program[36–38].

Further *ab initio* WFT calculations were performed using coupled-cluster theory at the CCSD(T) level, which used the B3LYP structures with retention of the molecular symmetries. In the CCSD(T) calculations, spin-restricted open-shell Hartree–Fock reference wavefunctions were used in the case of open-shell electron configurations. The CCSD(T) calculations were done using the frozen-core approximation with the $1s^2$ (O), $1s^22s^22p^6$ (Ar) and $5s^25p^6$ (Ir) orbitals excluded from the evaluation of the correlation energies. Stationary points on the potential energy surface were characterized by harmonic vibrational frequency calculations for both the ^{16}O and the ^{18}O isotopomers. For all other elements, the mass of the most abundant isotope was used in the CCSD(T) calculations. *Ab initio* coupled-cluster calculations were done using the CFOUR program package[39].

To better account for the non-dynamic electron correlation arising from electronic transitions from O 2*p* lone pairs to Ir 5*d* orbitals, we applied *ab initio* complete active space second-order perturbation theory (CASPT2), as implemented in MOLPRO 2008.1[40], to do ground-state geometry optimizations of the $[IrO_4]^+$ and $[IrO_4]^+\cdot$Ar cations using the same aug-cc-pVTZ(-PP) basis sets. In the CASPT2 calculations of $[IrO_4]^+$ with T_d symmetry, the active space contains the lowest five virtually occupied orbitals (that is, Ir–O antibonding orbitals of *e* and t_2 symmetry) and the highest six occupied orbitals of t_1 and t_2 symmetry (that is, non-bonding orbitals of O 2*p* character), which gives 12 electrons in 11 orbitals, that is, CAS(12, 11). Similar active spaces were chosen for $[IrO_4]^+\cdot$Ar isomers of C_{3v}, C_{2v} and C_s symmetry, respectively. A larger active space containing the lowest four unoccupied orbitals and all the occupied valence orbitals except the Ir non-bonding 5*d* orbital of a_1 symmetry and the O–O σ-bonding orbital of a_1 symmetry, which includes 20 electrons and 14 orbitals, that is, CAS(20, 14) was chosen for the $[(O_2)IrO_2]^+$ cation with C_{2v} symmetry. In CASPT2 calculations, the $1s^2$ (O), $1s^22s^22p^6$ (Ar) and $5s^25p^6$ (Ir) orbitals were not correlated, to save computing time.

Assignment of oxidation states. Usually the formal oxidation state of a central atom in a coordination sphere is defined as the charge of the central atom when every ligand of the coordination sphere is removed in its most stable form. The bonding electron pairs between the metal centre and the ligands are therefore exclusively assigned to the more electronegative fragment, resulting in negative oxidation states. For instance, for fluorine and doubly bonded oxygen ligands the oxidation states of fluorine and oxygen are −I and −II, respectively. According to these rules, the oxidation number of iridium in the $[IrO_4]^+$ cation is IX, whereas for the isoelectronic OsO_4 molecule, an oxidation state of VIII is obtained for osmium. However, the concept of oxidation states is a formal one and it has to be kept in mind that calculated atomic charges cannot be used to directly determine oxidation numbers[4]. The former mostly depend on the electronegativities of the ligands and not on the oxidation state of the metal, as exemplified by the isoelectronic d^0 anions $[V^{V}O_4]^{3-}$, $[Cr^{VI}O_4]^{2-}$ and $[Mn^{VII}O_4]^{-}$, which all represent the highest possible oxidation states of the metal elements, namely V, VI and VII, and for which almost identical charges of 1.05, 1.09 and 0.96 were computed for the central atoms[4,41]. We note that the computed charge of Cr(VI) is, in fact, higher than that of Mn(VII) (refs 4, 41). The calculated atomic charges at the B3LYP/aug-cc-pVTZ(-PP) level using natural population analyses of osmium and iridium in OsO_4 and $[IrO_4]^+$ are 1.475 and 1.470, respectively. These atomic charges amount to only a small fraction of the formal oxidation state, which is, however, well established in the case of $Os^{VIII}O_4$, and there is thus no doubt about the assignment of the formal oxidation state of $[Ir^{IX}O_4]^+$, even if the calculated charge of Ir(IX) is slightly less than that of Os(VIII).

23. Frisch, M. J. *et al.* Gaussian09, revision A.1 (Gaussian, Inc., 2009).
24. Becke, A. D. Density-functional exchange-energy approximation with correct asymptotic behavior. *Phys. Rev. A* **38,** 3098–3100 (1988).
25. Becke, A. D. Density functional thermochemistry. III. The role of exact exchange. *J. Chem. Phys.* **98,** 5648–5652 (1993).
26. Lee, C., Yang, W. & Parr, R. G. Development of the Colle-Salvetti correlation-energy formula into a functional of the electron density. *Phys. Rev. B* **37,** 785–789 (1988).
27. Riedel, S., Straka, M. & Kaupp, M. Validation of density functional methods for computing structures and energies of mercury(IV) complexes. *Phys. Chem. Chem. Phys.* **6,** 1122–1127 (2004).
28. Grimme, S., Antony, J., Ehrlich, S. & Krieg, H. A consistent and accurate ab initio parametrization of density functional dispersion correction (DFT-D) for the 94 elements H-Pu. *J. Chem. Phys.* **132,** 154104 (2010).
29. Kendall, R. A., Dunning, T. H. & Harrison, R. J. Jr. Electron affinities of the first-row atoms revisited. Systematic basis sets and wave functions. *J. Chem. Phys.* **96,** 6796–6806 (1992).
30. Woon, D. E. & Dunning, T. H. Jr. Gaussian basis sets for use in correlated molecular calculations. III. The atoms aluminum through argon. *J. Chem. Phys.* **98,** 1358–1371 (1993).
31. Peterson, K. A., Figgen, D., Dolg, M. & Stoll, H. Energy-consistent relativistic pseudopotentials and correlation consistent basis sets for the 4d elements Y–Pd. *J. Chem. Phys.* **126,** 124101 (2007).
32. Figgen, D., Peterson, K. A., Dolg, M. & Stoll, H. Energy-consistent pseudopotentials and correlation consistent basis sets for the 5d elements Hf–Pt. *J. Chem. Phys.* **130,** 164108 (2009).
33. Turbomole Version 6.2, http://www.turbomole.com (TURBOMOLE Gmbh, 2011).
34. Van Lenthe, E. & Baerends, E. J. Optimized Slater-type basis sets for the elements 1–118. *J. Comput. Chem.* **24,** 1142–1156 (2003).
35. Van Lenthe, E., Baerends, E. J. & Snijders, J. G. Relativistic regular two-component Hamiltonians. *J. Chem. Phys.* **99,** 4597–4610 (1993).
36. ADF v 2013.01, http://www.scm.com (SCM, 2013).
37. Fonseca Guerra, C., Snijders, J. G., Te Velde, G. & Baerends, E. J. Towards an order-N DFT method. *Theor. Chem. Acc.* **99,** 391–403 (1998).
38. te Velde, G. *et al.* Chemistry with ADF. *J. Comput. Chem.* **22,** 931–967 (2001).
39. Stanton, J. F. *et al.* CFour 1.2 ed., http://www.cfour.de (2010).
40. Werner, H.-J. MOLPRO version 2008. 1, http://www.molpro.net (2008).
41. Aullón, G. & Alvarez, S. Oxidation states, atomic charges and orbital populations in transition metal complexes. *Theor. Chem. Acc.* **123,** 67–73 (2009).